

# A synaptic input portal for a mapped clock oscillator model of neuronal electrical rhythmic activity

José Zariffa, Mark Ebden and Berj L Bardakjian

Institute of Biomaterials and Biomedical Engineering, Edward S Rogers Sr Department of Electrical and Computer Engineering, University of Toronto, Toronto, M5S 3G9 Canada

E-mail: berj@cbl.utoronto.ca

Received 28 May 2004

Accepted for publication 19 August 2004

Published 10 September 2004

Online at [stacks.iop.org/JNE/1/158](http://stacks.iop.org/JNE/1/158)

doi:10.1088/1741-2560/1/3/005

## Abstract

Neuronal electrical oscillations play a central role in a variety of situations, such as epilepsy and learning. The mapped clock oscillator (MCO) model is a general model of transmembrane voltage oscillations in excitable cells. In order to be able to investigate the behaviour of neuronal oscillator populations, we present a neuronal version of the model. The neuronal MCO includes an extra input portal, the synaptic portal, which can reflect the biological relationships in a chemical synapse between the frequency of the presynaptic action potentials and the postsynaptic resting level, which in turn affects the frequency of the postsynaptic potentials. We propose that the synaptic input–output relationship must include a power function in order to be able to reproduce physiological behaviour such as resting level saturation. One linear and two power functions (Butterworth and sigmoidal) are investigated, using the case of an inhibitory synapse. The linear relation was not able to produce physiologically plausible behaviour, whereas both the power function examples were appropriate. The resulting neuronal MCO model can be tailored to a variety of neuronal cell types, and can be used to investigate complex population behaviour, such as the influence of network topology and stochastic resonance.

## 1. Introduction

Simulations of electrical oscillations in neuronal populations have become ubiquitous in recent years, because of their central role in a variety of topics from epilepsy to brain–computer interfaces. Of course, any analysis of a network of neurons will depend on the mechanism used to connect cells to each other. Hence, many different descriptions of chemical synapses have been introduced, such as the ones by Liaw [1], Ermentrout [2], White [3], or Traub [4]. The synapse model cannot be separated completely from the cell model, so we must understand the latter before discussing the synapse. Here we are concerned with modelling cells with intrinsic oscillations, as opposed to using models that require external inputs or network interactions to produce rhythmic behaviour (for example variants of the Hodgkin–Huxley model such as [3, 5–9]). Several mathematical oscillators have been

proposed to describe cells with omnipresent rhythms [10–13], most of them based on Winfree's equations [14]. However, these models can usually only reproduce cell behaviour qualitatively, not quantitatively.

On the other hand, the mapped clock oscillator (MCO), first described by Bardakjian [15], is a multiportal generalization of the Winfree-type oscillator that is quantitative in nature and exhibits refractory properties. Its parameters can be obtained directly from the Fourier analysis of the measured intrinsic transmembrane voltage waveform of the uncoupled cell. Each oscillator consists of a dynamic nonlinearity that governs the two fundamental state variables of the system, and a static nonlinearity that maps those state variables onto the observable output (figure 1). The dynamic nonlinearity represents the clock mechanism of the oscillator. The values of its state variables are modified by three input 'portals', each of which corresponds to a different type of

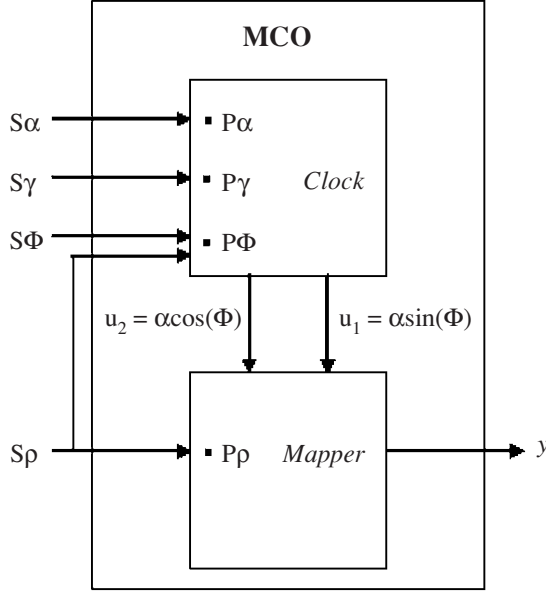


**Figure 1.** Mapped clock oscillator schematic.

coupling pathway (gap junctions, field effects and membrane receptors). The static nonlinearity represents the cellular membrane. It is this mapper (or transformer) that can be changed to represent the waveform of the specific cell being modelled. The MCO model has been previously used to model electrical oscillations in gut smooth muscle [15]. However, our recent studies have focused on neurons in the hippocampus and the surrounding regions. Therefore, the purpose of this study is to develop a neuronal MCO model. The improvements we aim to make deal mainly with adding a fourth input portal to model chemical synapses.

The simulations presented in this paper were all done using two unidirectionally coupled MCOs. The effects of both unidirectional and bidirectional coupling on the behaviour of the MCO (with three input portals) and its predecessors have been investigated in previous studies [11, 15–19].

## 2. Methods

The MCO model was created with the understanding that some excitable cells can undergo rhythmic transmembrane depolarizations. These nonlinear oscillators have an ‘intrinsic frequency’, but are influenced by their environment, including other nearby oscillators. Each oscillator has an ‘intrinsic clock’, described by two differential equations:

$$\dot{\alpha}_n = \omega_n \alpha_n (1 - \alpha_n^2) \quad (1)$$

$$\dot{\phi}_n = \omega_n \quad (2)$$

where  $\alpha_n$  is the amplitude,  $\phi_n$  is the phase and  $\omega_n$  is the intrinsic frequency of the clock output for the  $n$ th oscillator in a population of  $N$  oscillators. Transforming from polar to Cartesian coordinates using

$$u_{1n} = \alpha_n \sin(\phi_n) \quad (3)$$

$$u_{2n} = \alpha_n \cos(\phi_n) \quad (4)$$

and adding the effective stimuli ( $S_\alpha$ ,  $S_\phi$ ,  $S_{\gamma 1}$  and  $S_{\gamma 2}$ ) applied to the clock’s three input portals ( $P_\alpha$ ,  $P_\phi$  and  $P_\gamma$  in figure 1), we get the following dynamic nonlinearity:

$$\dot{u}_{1n} = \omega_n [u_{2n}(1 + S_{\phi n}) + u_{1n}(1 + S_{\alpha n} - u_{1n}^2 - u_{2n}^2)] + S_{\gamma 1n} \quad (5)$$

$$\dot{u}_{2n} = \omega_n [-u_{1n}(1 + S_{\phi n}) + u_{2n}(1 + S_{\alpha n} - u_{1n}^2 - u_{2n}^2)] + S_{\gamma 2n}. \quad (6)$$

In previous versions of this model [15], the Cartesian form was used, mainly for historical reasons (e.g. [20]). However, the polar form is more computationally efficient and is also more intuitive for a model whose central component is a clock. Therefore, in this study we will revert to the polar form. Converting the Cartesian form (including portals) to polar coordinates, and adding a refractoriness function, we obtain

$$\dot{\alpha}_n = \omega_n \alpha_n (1 + S_{\alpha n} - \alpha_n^2) + S_{\gamma 1n} \sin(\phi_n) + S_{\gamma 2n} \cos(\phi_n) \quad (7)$$

$$\dot{\phi}_n = \omega_n (1 + R_n(\phi_n) S_{\phi n}) + \frac{1}{\alpha_n} (S_{\gamma 1n} \cos(\phi_n) - S_{\gamma 2n} \sin(\phi_n)). \quad (8)$$

In this study,  $\dot{\phi}_n$  and  $\alpha_n$  are forced to be non-negative (i.e. negative values are set to zero). The state variables of the clock are then mapped onto an observable output,  $y_n$ , which is also affected by the effective stimulus ( $S_\rho$ ) applied to the mapper through its synaptic portal ( $P_\rho$  in figure 1):

$$y_n = a_{0n} (1 + S_{\rho n}) + \alpha_n \sum_{k=1}^K [a_{kn} T_k(\cos(\phi_n)) + b_{kn} \sin(\phi_n) U_{k-1}(\cos(\phi_n))] \quad (9)$$

where

- $y_n$  represents the transmembrane voltage.
- $a_{0n}$  is the intrinsic resting level.
- $a_{kn}$ ,  $b_{kn}$  are the Fourier coefficients of the waveform of the intrinsic oscillation.
- $T_k$  and  $U_k$  are the  $k$ th Tchebychev polynomials of the 1st and 2nd type, respectively.
- $k$  is the harmonic index. In this study,  $K = 500$ .
- $S_\alpha$ ,  $S_\phi$ ,  $S_{\gamma 1}$ ,  $S_{\gamma 2}$  and  $S_\rho$  represent the inputs to the four different portals of the oscillator. If the oscillator is uncoupled, then these are all zero.
- $R_n(\phi_n)$  is the refractoriness function, which ensures that the neuron stops being sensitive to frequency inputs while it is bursting. It is implemented as a highpass Butterworth function as shown in the following equation:

$$R_n(\phi_n) = \frac{1}{\sqrt{1 + \left(\frac{2\pi r}{\phi_n}\right)^{2N}}}. \quad (10)$$

In this study,  $r = 0.15$  and  $N = 10$ .

The Tchebychev polynomials are used in the static nonlinearity of the mapper because in the absence of any stimuli ( $S_\alpha = S_\phi = S_{\gamma_1} = S_{\gamma_2} = S_\rho = 0$ ) the resulting static nonlinearity reduces to a standard Fourier series [15]. The parameters of the static nonlinearity are the Fourier coefficients. Hence, the measured transmembrane voltage waveform of an uncoupled biological oscillator can be analysed in a Fourier series to determine the model parameters of the mapper. To determine the intrinsic parameters for this project, previously recorded data from a rat hippocampal slice were used [18]. The slice was bathed in a low-calcium medium, which greatly diminished the synaptic transmission between neurons, thereby eliminating the synaptic stimuli and moving the neurons closer to their intrinsic state. In this study, since the electrical recording from the hippocampal slice under low-calcium conditions was well characterized by a Fourier series, we may assume that it represents the output of an intrinsic MCO. Each MCO may represent either a single bursting neuron or a synchronous population of neurons, as long as the output can be characterized by a Fourier series.

Each of the four input portal stimuli  $S_x$  in (7)–(9) corresponds to a different type of biological stimulus or coupling, and therefore affects the model differently. The gap junction portal  $P_\gamma$  provides the means for direct interaction between the intracellular clock variables of coupled cells, thereby allowing for a context of continuity between the intracellular media of the two cells. The field coupling portal  $P_\phi$  provides the means for modifying the phase of the oscillations, allowing for a context of phase resetting of the clock [14]. The receptor portal  $P_\alpha$  provides the means for modifying the amplitude of the oscillation, allowing for a context of dose–response amplitude characteristics [14]. If the rate processes of the clock variables are represented in polar form (as described in [14, 15]), then it becomes apparent that the application of a stimulus through either the field coupling portal  $P_\phi$  or the receptor coupling portal  $P_\alpha$  would have a direct effect on the rate of change of either phase or amplitude, respectively. The synaptic coupling portal  $P_\rho$  provides the means for modifying the resting level in a postsynaptic cell according to the frequency of oscillations in a presynaptic cell, thereby providing for a context of frequency decoding by the synapse. Note that changes in resting level may in turn affect the postsynaptic frequency of oscillation by modifying the rate of change of the clock phase  $\dot{\phi}_n$ . In general, for the  $n$ th oscillator, having the set  $I_{nm}$  of neighbouring oscillators, the four input portals have the equations shown below in (11)–(15).

Portal  $P_\phi$ :

$$S_{\phi n} = \frac{\sum_{m \in I_{nm}} (c_{\phi nm} y_m) + a_{0n} S_{\rho n} + S_{\phi ne}}{\sigma_n} \quad (11)$$

Portal  $P_\alpha$ :

$$S_{\alpha n} = \frac{\sum_{m \in I_{nm}} (c_{\alpha nm} y_m) + S_{\alpha ne}}{\sigma_n} \quad (12)$$

Portal  $P_\gamma$ :

$$S_{\gamma 1n} = \frac{\sum_{m \in I_{nm}} (c_{\gamma nm} \alpha_m \sin(\phi_m)) + S_{\gamma ne}}{\delta_n} \quad (13)$$

$$S_{\gamma 2n} = \frac{\sum_{m \in I_{nm}} (c_{\gamma nm} \alpha_m \cos(\phi_m)) + S_{\gamma ne}}{\delta_n} \quad (14)$$

Portal  $P_\rho$ :

$$S_{\rho n} = f \left( \frac{\sum_{m \in I_{nm}} c_{\rho nm} \dot{\phi}_m + S_{\rho ne}}{\text{sgn}(a_{0n}) \omega_n} \right) \quad (15)$$

where

- $\sigma_n = (\sum_{k=1}^K (a_{kn}^2 + b_{kn}^2))^{1/2}$  is a normalization factor for the mapper, representing the amplitude of the intrinsic waveform.
- $\delta_n$  is a normalization factor for the clock.
- $\omega_n$  is the  $n$ th oscillator's intrinsic frequency.
- $c_\alpha, c_\phi, c_\gamma$  and  $c_\rho$  represent the coupling factors between the oscillators. They are real numbers between 0 and 1, where 1 implies that the corresponding portal is fully open, and 0 implies that it is closed. The sign of  $c_\rho$  is used to distinguish between excitatory and inhibitory synapses.
- $y_m$  is the transmembrane voltage of the driving oscillator.
- $S_{\alpha ne}, S_{\phi ne}, S_{\gamma ne}$  and  $S_{\rho ne}$  represent the extrinsic stimuli that are applied to the  $n$ th oscillator via the portals.
- The synaptic function  $f()$  is either (a) linear, (b) Butterworth-type or (c) sigmoidal.

### 2.1. The synaptic model

The input–output relationship of the synaptic portal  $P_\rho$  is a relationship between the presynaptic frequency ( $\dot{\phi}_m$ ) and the change in the postsynaptic potential ( $a_{0n} S_{\rho n}$ ). This postsynaptic potential change in turn modifies the postsynaptic frequency ( $\dot{\phi}_n$ ), as shown in (11) where  $S_\rho$  is included in the  $S_\phi$  expression. This is meant to reflect that postsynaptic depolarization (or hyperpolarization) will increase (or decrease) the postsynaptic frequency of oscillations. Since  $S_{\rho n}$  is a dimensionless quantity, it is multiplied by  $a_{0n}$  to give it units of voltage. A negative  $S_{\rho n}$  (which corresponds to a depolarizing effect because  $a_{0n}$  is negative for neurons at rest) increases  $S_{\phi n}$  and thus increases the postsynaptic frequency of oscillations. Similarly, a positive  $S_{\rho n}$  corresponds to a hyperpolarizing effect, decreases  $S_{\phi n}$  and decreases the postsynaptic frequency of oscillations.

The synaptic model is dependent on the synaptic function  $f()$ , so we will investigate three possible functions.

### 2.2. Linear synaptic function

The simplest choice is a linear function with two parameters  $\{v_1; v_2\}$ , as shown in (16). Our first set of simulations will therefore use this implementation,

$$f(x) = v_1 x + v_2. \quad (16)$$

### 2.3. Butterworth synaptic function

Next, we will consider a highpass Butterworth function with three parameters  $\{v_1; v_2; v_3\}$ . The general form of the function is given by the following equation:

$$f(x) = \frac{v_1 \text{sgn}(x)}{\sqrt{1 + \left[ \frac{v_2}{x \text{sgn}(x)} \right]^{v_3}}} \quad (17)$$

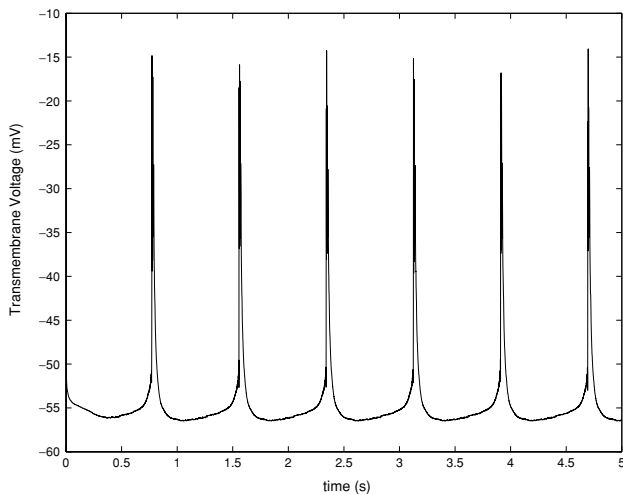


**Figure 2.** Output waveform of an unstimulated MCO.

#### 2.4. Sigmoidal synaptic function

Thirdly, because of the omnipresence of sigmoidal-type behaviours in neural networks, we choose a sigmoid function with three parameters  $\{\nu_1; \nu_2; \nu_3\}$ . The general form of the sigmoid is given by

$$f(x) = \nu_1 \left[ \frac{2}{1 + e^{(-\nu_2(x-\nu_3))}} - 1 \right]. \quad (18)$$

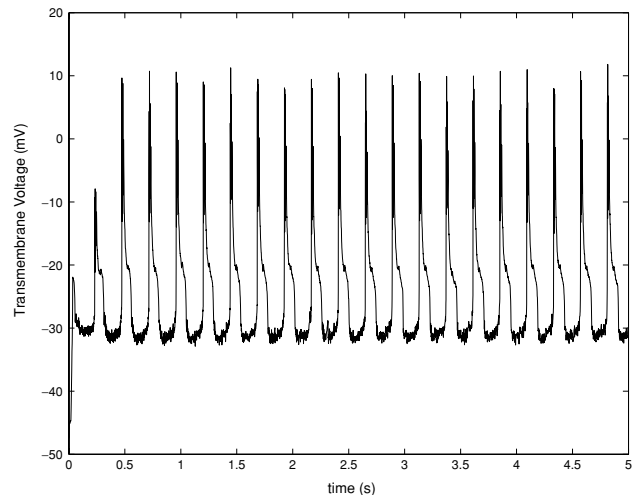
### 3. Results

Figure 2 shows the output of the MCO model in the absence of stimulation. The simulation quantitatively corresponds to the biologically recorded transmembrane voltage in CA3 pyramidal cells under low-calcium conditions, having an intrinsic frequency of 1.275 Hz [18]. The normalization factor  $\delta_n$  is set to 0.1, and there are no applied extrinsic stimuli. The differential equations were solved using numerical algorithms (BSODE) based on Gear's method [21–23]. Such a method can deal with stiff differential equations, hence it can successfully deal with all our simulation cases.

To illustrate the effects of the synaptic portal, two MCOs were unidirectionally coupled via  $P_\rho$  only. Both oscillators had the same intrinsic parameters as described above, with the exception of the intrinsic frequency of the driving MCO.

For a driving MCO frequency of 10 Hz, figures 3 and 4 show the outputs of the driven MCO when the synapse is excitatory and inhibitory, respectively. Both of these simulations used a Butterworth synaptic function with the parameter set  $\{\nu_1 = 1; \nu_2 = 9; \nu_3 = 4\}$ . Note that the postsynaptic frequency of the oscillations is affected as well as the resting level, because of the  $S_\rho$  term introduced into the expression for  $S_\phi$ . In the inhibitory case, the frequency is reduced so much that the MCO does not oscillate during the simulated time interval, but we could scale the effects through the choice of  $\nu_1$ .

Next, we compared the three types of synaptic functions using the above example with an inhibitory synapse between the two unidirectionally coupled MCOs. In the following



**Figure 3.** Output waveform of an MCO stimulated via the input portal  $P_\rho(c_\rho = 1)$ .

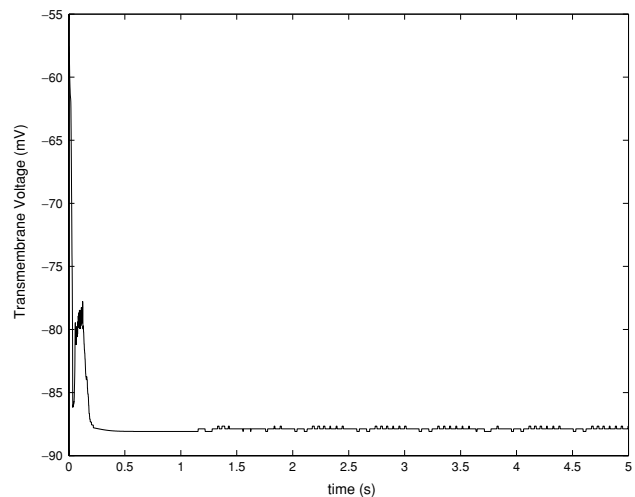


**Figure 4.** Output waveform of an MCO stimulated via the input portal  $P_\rho(c_\rho = -1)$ .

cases, the driving MCO frequency was swept from 1 to 35 Hz (in steps of 1 Hz between 1 Hz and 15 Hz, then in steps of 5 Hz between 15 Hz and 35 Hz). While all three synaptic functions will result in the type of behaviour shown in figures 3 and 4, the relationship between the presynaptic bursting frequency and the postsynaptic resting level (and hence frequency) will be different, as shown in the following sections.

To determine the parameter sets of the synaptic functions and compare the three types, a reference synaptic curve was selected. Since our mapper waveform was measured from rat CA3 hippocampal neurons, our synaptic function must be based on a resting level versus stimulation frequency plot corresponding to such a cell. We used the NEURON software package to obtain a simulated approximation of this plot. The cell model used was one developed by Migliore *et al* [24]. The parameter set  $(\nu_1; \nu_2; \dots)$  of each synaptic function was then chosen to model as closely as possible the same behaviour (range of resting levels and slope of the curve).

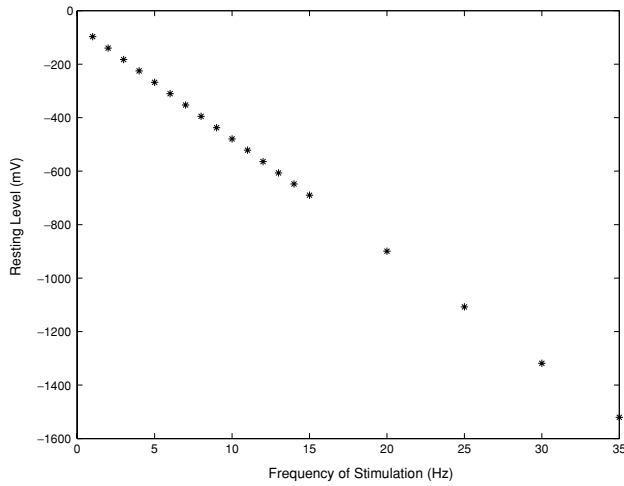


**Figure 5.** Resting level of the neuron's transmembrane voltage in response to pulse trains of synaptic stimulation, when the synaptic function is linear.

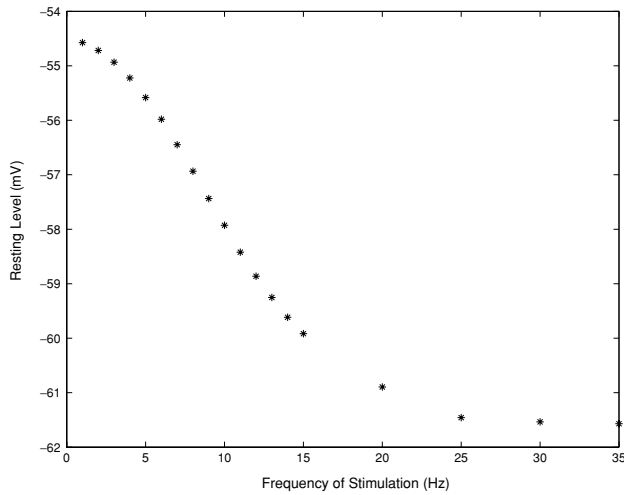


**Figure 6.** Resting level of the neuron's transmembrane voltage in response to pulse trains of synaptic stimulation, when the synaptic function is a Butterworth function.

We simulated each system for 20 s, which is enough for the resting level to stabilize. The resting level values reported in figures 5 to 10 are the average values of the resting level over the last 5 s of a given simulation. The postsynaptic resting level is given by  $a_0(1 + S_\rho)$ .

### 3.1. Linear synaptic function

For a linear synaptic function with the parameter set  $\{v_1 = 1; v_2 = 0\}$ , the relationship between frequency of stimulation and resting level is shown in figure 5, for an inhibitory synapse. Clearly, the linear function is inappropriate for modelling the physiological behaviour.

### 3.2. Butterworth synaptic function

For a Butterworth synaptic function with the parameter set  $\{v_1 = 0.13; v_2 = 9; v_3 = 4\}$ , the relationship between

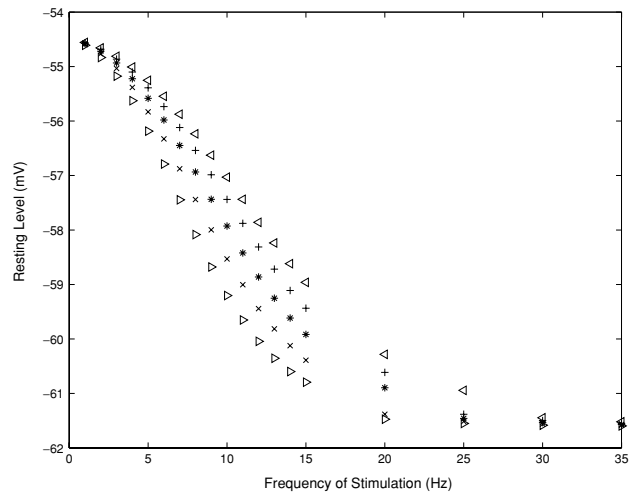


**Figure 7.** Resting level of the neuron's transmembrane voltage in response to pulse trains of synaptic stimulation, when the synaptic function is a Butterworth function with  $v_3 = 4$  and  $v_2 = 7(>)$ , 8 ( $\times$ ), 9 (\*), 10 (+) and 11 (<).

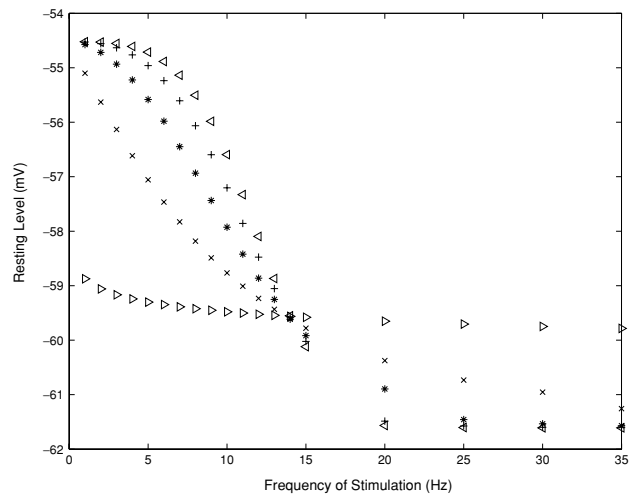


**Figure 8.** Resting level of the neuron's transmembrane voltage in response to pulse trains of synaptic stimulation, when the synaptic function is a Butterworth function with  $v_2 = 9$  and  $v_3 = 0.2(>)$ , 2 ( $\times$ ), 4 (\*), 6 (+) and 8 (<).

frequency of stimulation and resting level is shown in figure 6, for an inhibitory synapse. Figure 7 shows how the relationship varies when the  $v_2$  parameter of the Butterworth function changes, and figure 8 shows how it varies when the parameter  $v_3$  changes. The results suggest that this function is appropriate for modelling physiological behaviour.

### 3.3. Sigmoidal synaptic function

For a sigmoidal synaptic function with the parameter set  $\{v_1 = 0.13; v_2 = 0.23; v_3 = 2\}$ , the relationship between frequency of stimulation and resting level is shown in figure 9, for an inhibitory synapse. Figure 10 shows how the relationship varies when the  $v_2$  parameter of the sigmoid

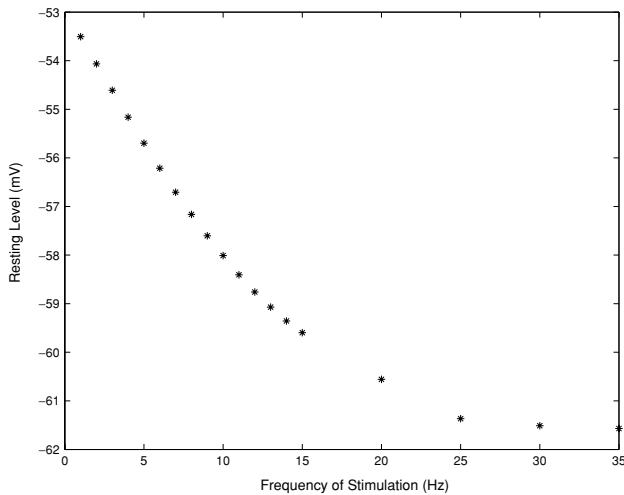


**Figure 9.** Resting level of the neuron's transmembrane voltage in response to pulse trains of synaptic stimulation, when the synaptic function is a sigmoid.

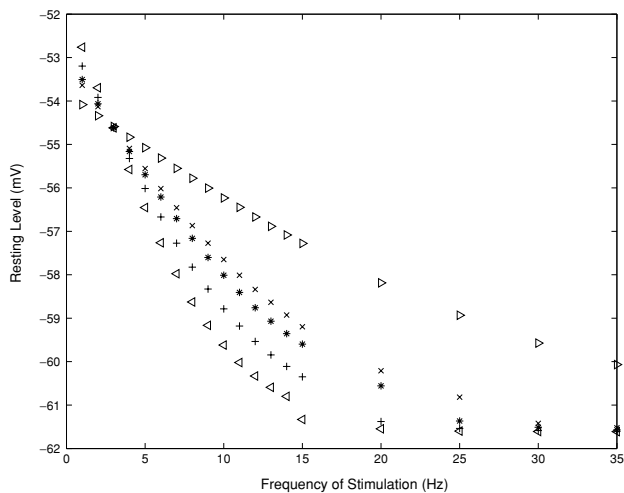


**Figure 10.** Resting level of the neuron's transmembrane voltage in response to pulse trains of synaptic stimulation, when the synaptic function is a sigmoid with  $\nu_2 = 0.1 (>)$ ,  $0.2 (x)$ ,  $0.23 (*)$ ,  $0.3 (+)$  and  $0.4 (<)$ .

changes. The results suggest that this function is also appropriate for modelling physiological behaviour.

#### 4. Discussion and conclusions

The output of each MCO closely matches the biological intrinsic oscillations measured under low-calcium conditions (low-complexity modes of behaviour). Populations of coupled MCOs were shown by our group [13, 18, 19, 25, 26] to display biological characteristics under both normal calcium conditions (high-complexity modes of behaviour [13, 18, 26]) and low-magnesium conditions (spontaneous seizure-like activity [19, 25]). Applications of coupled MCO models included influence of topology on complexity [26], stochastic resonance and coherence [13]. The neuronal MCO allows us to simulate the behaviour of oscillator neurons, but more

importantly it allows us to study networks of these cells. The main strength of the model is not just how well it reproduces the output of a single isolated cell, but rather how precisely it can describe the coupling between such cells. By having separate mechanisms for each possible type of coupling (electrical, chemical, or field-based), we can better understand the influence of each of them on population behaviours such as entrainment, contact inhibition, or the appearance of high-complexity (possibly chaotic) dynamics. This is an essential feature for any neuronal model, since the CNS relies at its most basic level on interactions amongst a vast number of neurons. The presence of gap junctions and field effects in the neuronal population has been shown to have a significant role to play (e.g. [27, 28]), and so it is important to be able to simulate their effects explicitly. Of course, the preponderance of synaptic connections is undeniable, which is why the more realistic and flexible synapse implementation introduced in this paper is important for the validity of the MCO model.

The linear version of the synaptic function results in a MCO resting level that is directly proportional to the frequency of applied action potentials. Saturation cannot be achieved without introducing some other mechanism, such as feedback. In the absence of saturation, the resting levels achieved (for example  $-1600$  mV) are clearly not plausible, making the linear synaptic function inappropriate for the simulation of physiological data. With the two nonlinear functions, on the other hand, we were able to achieve neuronal resting level saturation without having recourse to any extra mechanisms. These function types (highpass Butterworth and sigmoid) can therefore be used to realistically model physiological data. From a computational perspective, the highpass Butterworth function may run into numerical difficulties since it includes a variable argument which is raised to a power. Because of the large range of values of  $\frac{\nu_2}{x}$ , the raising to the power  $\nu_3$  can lead to overflow or underflow conditions associated with computer accuracies. This is avoided in the sigmoidal function.

A mapping between the presynaptic frequency and the postsynaptic frequency was achieved via two processes. First, the relationship between presynaptic frequency and postsynaptic resting level was modelled using a static nonlinearity (a saturating synaptic function such as a highpass Butterworth or a sigmoid function). Second, the relationship between the postsynaptic resting level and the postsynaptic frequency was modelled using a dynamic nonlinearity (the clock mechanism in the MCO).

#### Acknowledgments

This work has been supported by the Natural Sciences and Engineering Research Council of Canada (NSERC) and the 'Fonds québécois de recherche sur la nature et les technologies'.

#### References

- [1] Liaw J and Berger T W 1999 Dynamic synapse: harnessing the computing power of synaptic dynamics *Neurocomputing* **26–27** 199–206

- [2] Ermentrout B 2003 Dynamical consequences of fast-rising, slow-decaying synapses in neuronal networks *Neural Comput.* **15** 2483–522
- [3] White J A, Chow C C, Ritt J, Soto-Trevino C and Kopell N 1998 Synchronization and oscillatory dynamics in heterogeneous, mutually inhibited neurons *J. Comput. Neurosci.* **5** 5–16
- [4] Traub R D, Whittington M A, Colling S B, Buzsáki G and Jefferys J G R 1996 Analysis of gamma rhythms in the rat hippocampus *in vitro* and *in vivo* *J. Physiol.* **493** 471–84
- [5] Plant R E and Kim M 1976 Mathematical description of a bursting pacemaker neuron by a modification of the Hodgkin–Huxley equations *Biophys. J.* **16** 227–44
- [6] Lee Y S, Chay T R and Ree T 1983 On the mechanism of spiking and bursting in excitable cells *Biophys. Chem.* **18** 25–34
- [7] Chay T R 1990 Bursting excitable cell models by a slow calcium current *J. Theor. Biol.* **142** 305–15
- [8] Ermentrout G B and Kopell N 1998 Fine structure of neural spiking and synchronization in the presence of conduction delays *Proc. Natl Acad. Sci. USA* **95** 1259–64
- [9] Ermentrout B, Pascal M and Gutkin B 2001 The effects of spike frequency adaptation and negative feedback on the synchronization of neural oscillators *Neural Comput.* **13** 1285–310
- [10] Kopell N and Ermentrout G B 1986 Subcellular oscillations and bursting *Math. Biosci.* **78** 265–91
- [11] Bardakjian B L, Sarna S K and Diamant N E 1990 Composite synthesized relaxation oscillators: application to modeling of colonic electrical control and response activity *J. Gastrointest. Motil.* **2** 109–16
- [12] Ermentrout G B and Kopell N 1991 Multiple pulse interactions and averaging in systems of coupled neural oscillators *J. Math. Biol.* **29** 195–217
- [13] Chiu A W L and Bardakjian B L 2004 Stochastic and coherence resonance in an in-silico neural model *Ann. Biomed. Eng.* **32** 732–43
- [14] Winfree A T 2001 *The Geometry of Biological Time* 2nd edn (New York: Springer)
- [15] Bardakjian B L and Diamant N E 1994 A mapped clock oscillator model for transmembrane electrical activity in excitable cells *J. Theor. Biol.* **166** 225–35
- [16] Bardakjian B L and Sarna S K 1980 A computer model of human colonic electrical control activity (ECA) *IEEE Trans. Biomed. Eng.* **27** 193–202
- [17] Bardakjian B L, El-Sharkawy T Y and Diamant N E 1983 On a population of labile synthesized relaxation oscillators *IEEE Trans. Biomed. Eng.* **30** 696–701
- [18] Bardakjian B L, Aschenbrenner-Scheibe R, Perez-Velazquez J L and Carlen P L 1995 Transmembrane voltage oscillations in CA3 neurons *Proc. 17th Int. Conf. IEEE/EMBS, Montreal, Quebec, 20–23 Sept.* pp 1503–4
- [19] Chiu A W L and Bardakjian B L 2004 Control of state transitions in an in-silico model of epilepsy using small perturbations *IEEE Trans. Biomed. Eng.* **51** at press
- [20] Minorsky N 1962 *Nonlinear Oscillations* (Princeton, NJ: Van Nostrand)
- [21] Gear C W 1971 *Numerical Initial Value Problems in Ordinary Differential Equations* (Englewood Cliffs, NJ: Prentice-Hall)
- [22] Parker T S and Chua L O 1989 *Practical Numerical Algorithms for Chaotic Systems* (New York: Springer)
- [23] Radhakrishnan K and Hindmarsh A C 1993 Description and Use of LSODE, the Livermore Solver for Ordinary Differential Equations NASA Reference Publication 1327 *Lawrence Livermore National Laboratory Report*
- [24] Migliore M, Cook E P, Jaffe D B, Turner D A and Johnston D 1995 Computer simulations of morphologically reconstructed CA3 hippocampal neurons *J. Neurophysiol.* **73** 1157–68
- [25] Bardakjian B L and Courville A 2000 Chaosmakers: Rhythm breakers *Proc. 2nd Int. ICSC Symp. on Neural Computation (NC'2000)* (Berlin, Germany, 23–26 May) pp 121i–v
- [26] Zariffa J and Bardakjian B L 2004 Topology and complexity in coupled mapped clock oscillators representing CA3 neural networks *Proc. BMES 2004 Annual Fall Meeting* (Philadelphia, PA, 13–16 Oct.)
- [27] Draguhn A, Traub R D, Schimtz D and Jefferys J G R 1998 Electrical coupling underlies high-frequency oscillations in the hippocampus *in vitro* *Nature* **394** 189–92
- [28] Faber D S and Korn H 1989 Electrical field effects: their relevance in central neural networks *Physiol. Rev.* **69** 821–63